Available online at www.sciencedirect.com

ScienceDirect

Procedia Structural Integrity 21 (2019) 120–129

Structural Integrity Procedia

www.elsevier.com/locate/procedia

1st International Workshop on Plasticity, Damage and Fracture of Engineering Materials

Investigation of Portevin-LeChatelier Bands in 5754 Aluminum Alloy under Various Strain Paths

O. Berk Aytuna[a], Mert Efe[a]*

[a]*Department of Metallurgical and Materials Engineering, Middle East Technical University, Ankara 06800, Turkey*

Abstract

This work investigated the mechanical and microstructural effects of Portevin-LeChatelier bands in aluminum 5754 alloy under different loading conditions. For these conditions (equibiaxial and uniaxial), an in-plane biaxial test apparatus was utilized with a miniature cruciform specimen. The amount and magnitude of load jumps and drops (serrations) due to the PLC bands were monitored by load cells and strain distributions were measured by digital image correlation technique. Under biaxial stretching, PLC bands nucleated and propagated repeatedly at the same region of the sample, while their formation was random under uniaxial tension. Overall contribution of PLC strain to the total strain was higher under equibiaxial stretching, yet there were no visible shear bands as the PLC bands were suppressed. Conversely, the shear stress state in tension promoted PLC bands and evolved them into sharp shear bands. Texture analysis confirmed the emergence of shear components and cube texture with increasing strain. The eventual failure of the sample was from the shear band(s). The main benefit of biaxial loading was prevention of undesired fracture from shear bands, without changing the overall forming characteristics and the initial copper texture of the material.

Peer-review under responsibility of the 1st International Workshop on Plasticity, Damage and Fracture of Engineering Materials organizers

Keywords: PLC; Cruciform; DIC; Biaxial; Forming

* Corresponding author. Tel.:+90-312-210-5925; fax:+90-312-210-2518.
E-mail address: mefe@metu.edu.tr

Peer-review under responsibility of the 1st International Workshop on Plasticity, Damage and Fracture of Engineering Materials organizers
10.1016/j.prostr.2019.12.093

1. Introduction

Portevin-Le Chatelier bands are unique plastic instabilities observed mostly in alloys having solute atoms. Al-Mg alloys are common examples showing deformation behavior based on the PLC bands. Presence of solute Mg atoms and their interaction (breakaway and pinning) with the mobile (gliding) dislocations or other obstacles causes dynamic strain aging in micro-scale (Cottrell (1953), Hertzberg and Hauser (2010), McCormick (1971); Mulford and Kocks (1979), Sleeswyk (1958)). At macro scale, the PLC bands appear as angled and narrow strain localized lines during plastic deformation (Shibkov et al. (2018), Yilmaz (2011)). PLC bands cause heterogenous deformation as a result of stress and strain jumps (serrations in flow curves) and the consequence is undesired visual sharp surface irregularities (shear bands) that can act as a stress concentrator for the catastrophic failures (Beaudoin et al. (2005), Shuklinov et al (2011), Yuzbekova et al. (2017)). Since 5xxx Al alloys are used in the automotive industry due to its sufficient strength, good formability and good corrosion characteristics (Hirsch and Al-Samman, (2013)), irregularities that affect these properties i.e. poor surface finish after shaping operations should not be desirable. On the other hand, dynamic strain aging phenomena leads to negative strain rate sensitivity (Antolovich and Armstrong (2014)) which affects the mechanical response of Al-Mg alloys negatively during shaping and complicates the optimization of shaping parameters.

PLC band characteristics basically depend on two factors; strain rate (Jiang et al. (2007)) and temperature (Chatterjee et al. (2011)). Variation of these two factors results in different sequence of nucleation and propagation of PLC bands such as continuous (type A), discontinuous (type B) or random (type C) (Ait-Amokhtar and Fressengeas (2010)). Factors apart from strain rate and temperature; grain size (Yuzbekova et al. (2017)), precipitates (Wen et al. (2005), heat treatment (Tian et al. (2018)), surface irregularities (Shuklinov et al, (2011)) or specimen shapes (Clausen et al. (2004)) also affects the PLC formation in Al-Mg alloys. Nonetheless, most of the previous studies used uniaxial loading (Ait-Amokhtar and Fressengeas (2010), Chatterjee et al. (2011), Clausen et al. (2004), Jiang et al. (2006, 2007), Saad et al. (2010); Tian et al. (2018), Wen et al. (2005)) to understand the deformation characteristics. Few studies in the literature focused on the PLC bands under different strain paths. These studies include observation of PLC band formation region with hydraulic bulge testing (Min et al. (2015)), yield loci or yield surface of Al-Mg alloys (Hamasaki and Tamashiro (2018), Iadicola et al. (2011)), PLC band detection with thermal observation techniques instead of digital image correlation (Le Cam et al. (2017)), forming and fracture strains of Al-Mg alloys (Song et al. (2016)) or hardening behavior and serration types under uniaxial, plain strain and biaxial condition (Houet al. (2018)). However, a systematic study under various strain paths is needed for the detailed characterization of the shape and contribution of individual PLC bands and their effects on the fracture and deformation mode. It is well known that under uniaxial loading, fracture occurs from localized shear bands (Motsi et al. (2014), Shibkov et al. (2018), Shuklinov et al. (2011), Zhemchuzhnikova et al. (2018)). The shear stress state under uniaxial tension is responsible from this and it may also affect the PLC band formation. There is no shear stress under biaxial tension, on the other hand, and the PLC formation may be different than the uniaxial.

In this work, the behaviour of PLC bands in Al-Mg alloy was investigated under uniaxial and equibiaxial condition in order to test the effect of strain path on their formation. An in-plane biaxial testing apparatus with strain analysis capability was utilized for this purpose. Firstly, shape of the bands and strain amount in the bands were analyzed with the DIC technique. Digital image correlation technique as an optical method could analyse spatio-temporal characteristics of these bands by displaying strain field of focused region (commonly gage length). When the PLC band nucleates at any area in that region, the strain distribution map has angled strain localized band(s) (generally 50^{o}-60^{o} to the tensile axis) (Cai et al. (2016), Sene et al. (2018)). This certain bands could provide information about nucleation or propagation characteristics of PLC bands depending on adjusted fps of CCD cameras. In other words, the type of propagation (A, B or C) could be described. After observing connections of PLC bands and the deformation mode characteristics of material under different loading conditions, PLC band contribution to the failure was established. Finally, texture evolution during deformation was investigated under the different strain paths and PLC conditions to investigate their combined effects on the final texture, which is a critical feature controlling the overall formability of Al sheets.

2. Experimental Procedure

2.1. Sample preparation

The material studied in this investigation was commercially produced Aluminum 5754-H111 alloy. The chemical composition of the material is given in Table 1. It was received in rolled-sheet form having 2 mm thickness, 1000 mm width and 2000 mm length. The material had uniform microstructure (Fig. 1a) with an average grain size of 10.3 ± 1.3 μm. Hardness of the material taken from the surface was 62.2 ± 2. kg/mm^2 and homogenous along the sheet. Material initially had Copper {112} <111> texture which is typical of rolled aluminum sheets (Fig. 1b. and Fig. 1c.).

Table 1. Weight percentages of elements in 5754 Aluminum alloy.

Al	Mg	Fe	Si	Mn	Zn	Cu	Sn	Ti	V	Ga
Balanced	2.88	0.4	0.39	0.14	0.1	0.06	0.03	0.02	0.02	0.01

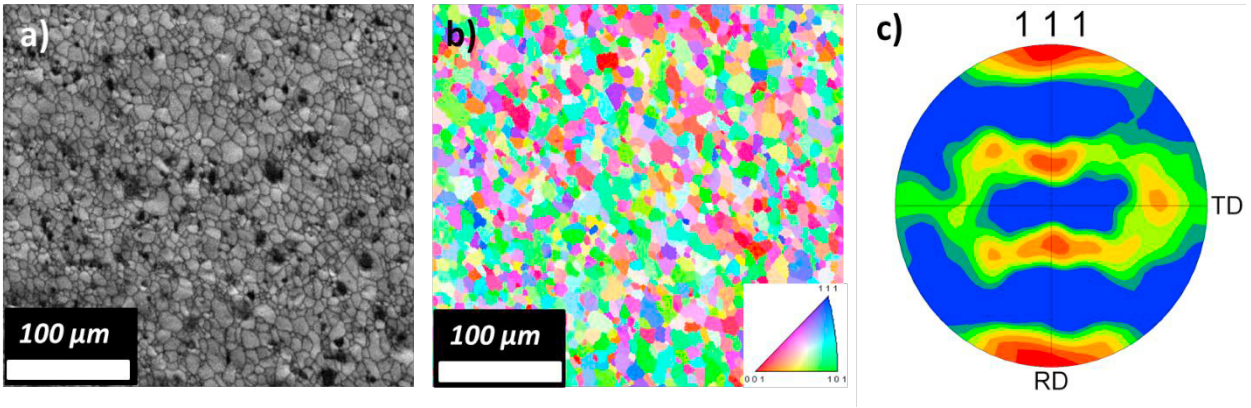

Fig 1. EBSD analysis of as-received Aluminum sheet showing (a) microstructure (b) grain orientation map (c) 111 pole figure.

Cruciform shaped sample used in testing was cut by water-jet from the rolled sheet and geometry of the sample is given in Fig. 2a. Detailed design of the sample were reported elsewhere by Seymen et al. (2016). CNC milling was used to obtain the reduced cross-section (pit) located in the middle of the geometry. The pit region was electropolished with Struers Lectropol-5 device with Struers A2solution (90 ml distilled water, 730 ml ethanol, 100 ml butoxyethanol and 78 ml perchloric acid). Electropolishing was done at 38 Volts for 30 seconds. Purpose of electropolishing was to reduce the surface roughness and eliminate the surface irregularities formed during milling.

2.2. In-plane biaxial testing and digital image correlation setup

The portable biaxial testing apparatus was assembled to a Shimadzu Bending Test Machine (capacity of 10kN) given in Fig. 2b. Apparatus converts the vertical load to horizontal loads along four arms and arms have same length to distribute the forces equally (Fig. 2c). Load cells recording data every 6 sec were attached to the arms and load difference at each arm does not exceed 100 N during the test. For uniaxial testing, two arms of the specimen along the rolling direction were attached to the apparatus whereas for equibiaxial testing, all arms of the specimen were attached. The experiments were repeated 4 times for equibiaxial, 6 times for uniaxial condition and the load-strain results given in the text are the representative behavior of all the tests. For the spatio-temporal characterization of the PLC bands, almost 100 separate bands were analyzed in a selected test of each condition.

Digital image correlation setup (Fig. 2d) consists of Basler piA2400-17gm GigE camera (5 MP resolution) with Sony ICX625 CCD sensor, Navitar Ultra Zoom 6000 zoom lens (1.40X-9.00X and NA=0.023-0.071, respectively) with co-axial LED illumination and 2X adapter, and a manual microstage. The setup was placed in order to monitor the 2 mm diameter pit (middle) region of the cruciform sample. 2.9x2.2 mm^2 field-of-view was obtained at 1.4X

magnification with 2448x2050 pixels resolution. Acrylic paint (diluted with acetone) was sprayed to the monitored region with airbrush for these magnifications. Spraying achieved the proper speckle pattern and contrast for DIC with average 25 μm black speckles on electropolished shiny surface. The recording rate varied from 1 fps (for spatial analysis) to 5 fps (for temporal analysis).

Matlab based 2D digital image correlation software Ncorr v1.2 was used to analyze strain distribution of the monitored region. Strain resolutions were 1.08 μm and 5.05 μm for 3X and 1.4X magnification, respectively. Error calculated by translation experiments was 0.14% for these magnifications. All images recorded with 5 fps rate were used to obtain strain-time graphs whereas consecutive images recorded with 1 fps rate were used to obtain spatial analysis of PLC bands. Median strain values were collected to plot strain-time graphs. Software calculated strains as Green-Lagrangian strains in x and y direction and they were converted to the true strain with the formula of $\varepsilon = \ln(\sqrt{2E+1})$ where ε is true strain and E is Green-Lagrangian strain. Moreover, equivalent strain calculation was done by: $\varepsilon\_eq = \sqrt{2/3(\varepsilon\_xx^2 + \varepsilon\_yy^2 + \varepsilon\_zz^2)}$. Strain in thickness was obtained by assuming that summation of strains in three axes equals to zero.

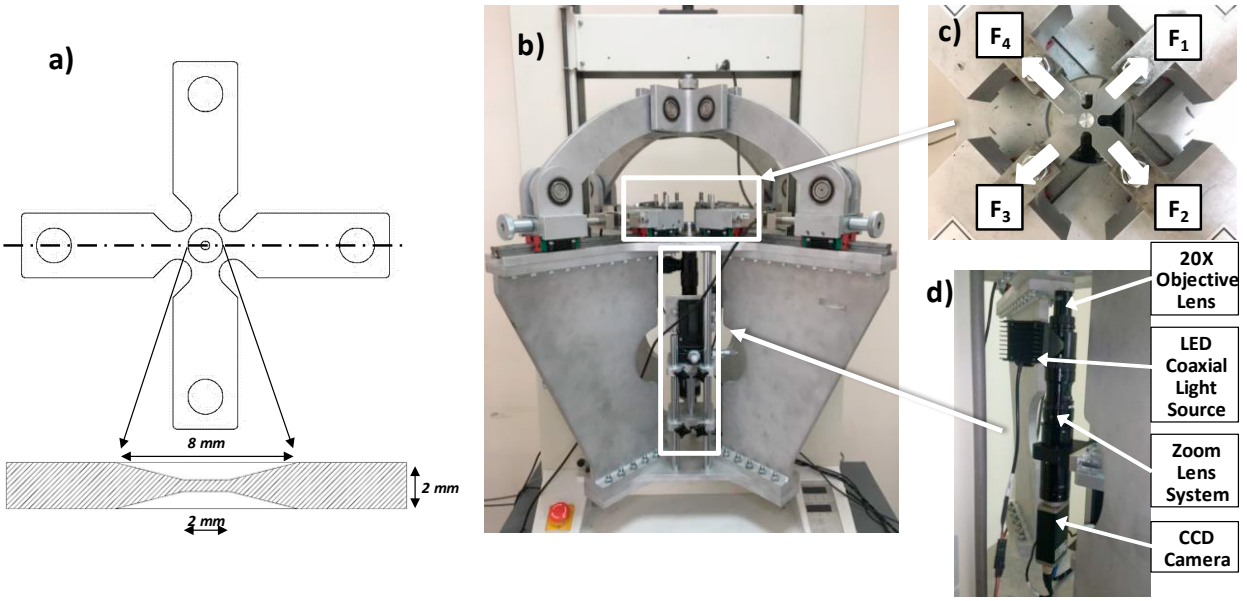

Fig 2. (a) Specimen geometry, (b) portable biaxial testing apparatus, (c) specimen attached to apparatus arms (d) DIC imaging unit.

2.3. Scanning electron microscopy and electron backscatter diffraction (EBSD)

FEI Nova Nano SEM 430 field emission scanning electron microscope at 18 kV accelerating voltage was used to monitor the surface irregularities, defects, slips and micro cracks after testing and to analyze fracture surfaces. EDAX EBSD camera equipped to SEM obtained the diffraction data with the software of Orientation Imaging Microscopy (OIM) Data Collector. OIM Analysis software was used to plot orientation maps and pole figures. Larger areas such as 450x450 μm^2 were studied for the representative pole figures. Standard cleanup procedures were applied in this software. Sample preparation for EBSD was done with the same electropolishing parameters and solution.

3. Results and Discussions

Fig. 3 shows differences in load response of the material under uniaxial and biaxial loading. Load-time graphs in Fig. 3a were converted to load-strain graphs in Fig. 3b by finding the strain values from DIC analysis at a given time. It was not possible to convert the load values to stresses as it was hard to measure reduction in the cross-section area. The load increase behavior is similar for both conditions (Fig. 3a). Materials deform with almost same hardening rate, yet the sample under biaxial tension fails at 0.34 equivalent strain (Fig. 3b). After this point, the material under uniaxial stretching continues to deform up to approximately 700 s, corresponding to an equivalent strain of 0.70 until fracture (Fig. 3b). Material shows no localized neck region and there is no remarkable load drop at fracture under both conditions due to nature of the biaxial testing apparatus and specimen design as explained in elsewhere (Güler and Efe (2018)). While material undergoes additional deformation under uniaxial loading, serrations of the curve due to the PLC effect seem to be more distinct in uniaxial case. Observed serration numbers under uniaxial loading are five times higher than that of under biaxial loading. Average load jump and drop amount is approximately 15 N for biaxial stretching, whereas it is 23 N for uniaxial stretching. Uniaxial condition leads to higher load jumps and drops during deformation. The first observed PLC band (serration) is seen at earlier stages (at time nearly 180 s) of the testing under uniaxial loading. Furthermore, there are no strict sequence of load jumps and drops with respect to time, indicating that the characteristics of the PLC bands are near to the Type C.

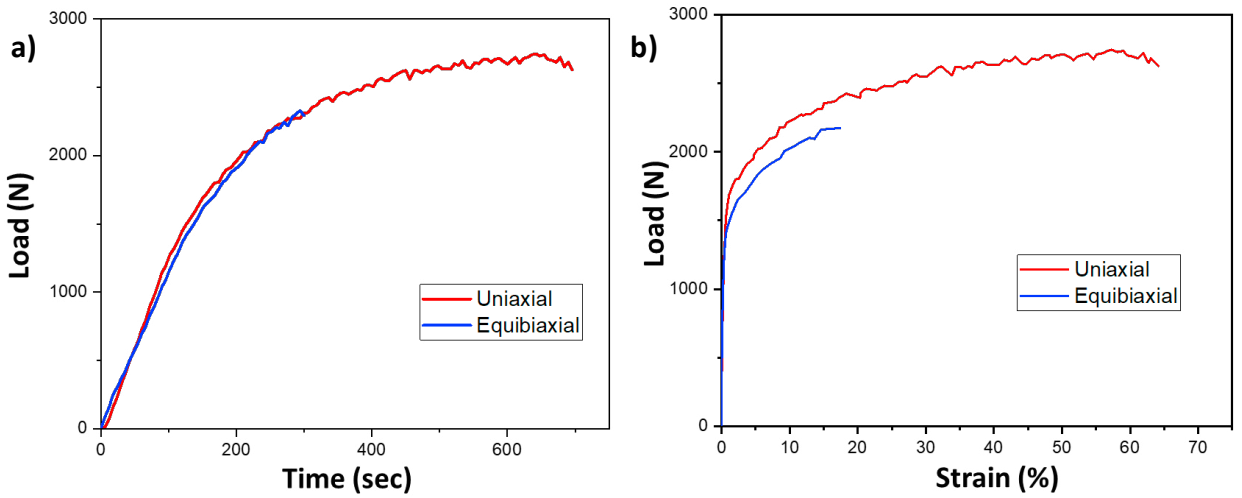

Fig. 3. (a) Load versus time graph (b) Load versus strain graph of the material during uniaxial and equibiaxial loading

2D DIC analysis gives the shape and strain amount in the PLC band by calculating strain distribution of the pit region by taking two consecutive images at each load jump and drop during the test. The DIC results (ε_{xx} direction) in Fig. 4a. are taken from different load jumps and drops during uniaxial tension. Red and yellow regions in the figure show strain localized regions. Shape of the PLC bands is sharp and distinct under uniaxial stretching, it also has an angle of 50° to the loading direction. The blue regions represent nearly strain-free regions and approximately half of the total area is strain-free; therefore, the deformation of the material is heterogeneous, where the strain is localized only in the PLC bands. Strain calculated in the PLC band from beginning to end of the test differs by 0.015 and the maximum strain is 0.026. Load increase during the test is responsible from the strain increase in the formed PLC bands. Also, multiple PLC bands can form at the same time, and these bands can either cross or be parallel to each other. The width of the bands differs from 150 μm to 400 μm. The strain distribution of individual PLC band has higher values through the centerline of the band and the strain usually peaks at one end of the centerline. The PLC bands are also repetitive; they can from at the same region at any time. However, nucleation and propagation of the bands do not have a sequence and they appear to be completely random.

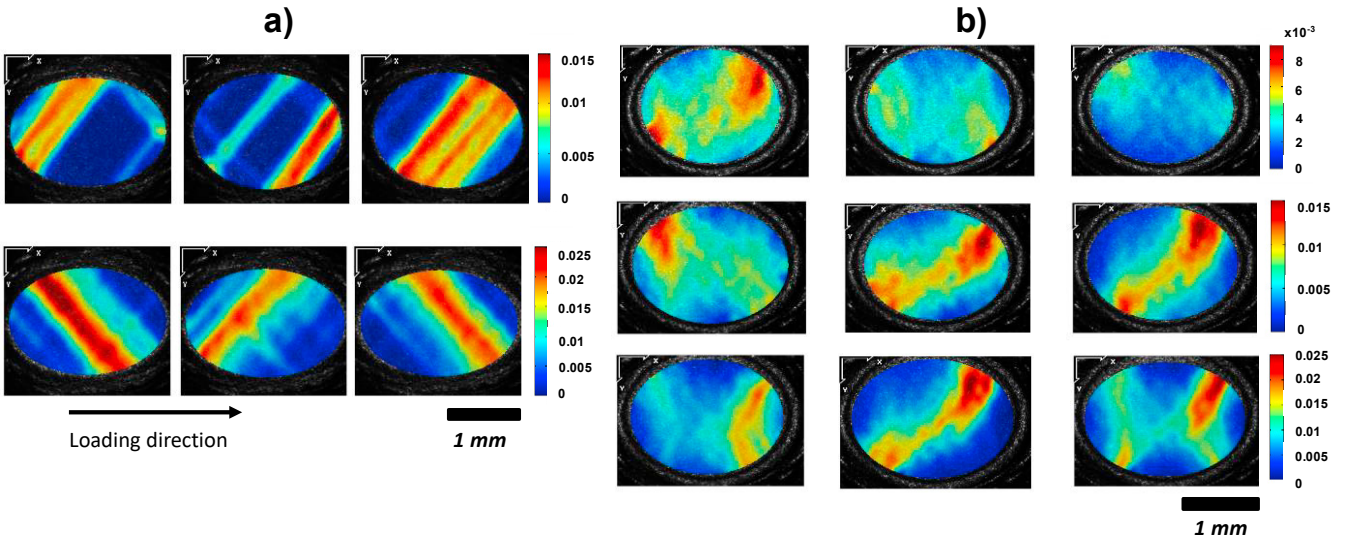

Fig. 4. Strain distribution map of the material from different time intervals (a) under uniaxial condition (b) under equibiaxial condition.

DIC results in ε_{xx} direction of deformation during biaxial testing of the material show different strain distribution compared to uniaxial testing (Fig. 4b). Instead of sharp, pronounced, and angled bands, there are diffuse and shifted bands formed under biaxial stretching. In this case, the strain-free blue regions cover approximately one third of the gage area. Strain values have a peak at the edge region as in uniaxial condition. However, the strain is not localized along the centerline of the PLC bands. The strain is lower in the middle of the pit region compared to the edge regions. Previous work on the testing apparatus (Seymen et al. (2016) showed that shear strain is negligible at the center region having 1 mm diameter during biaxial stretching. Coincidentally, the continuity of the PLC band is disrupted at the same region where there is no shear strain, indicating that the shear strain is critical in the formation of bands. Towards the end of the test, two PLC bands cross each other, which is visible by X shape in the strain maps (Fig. 4b). Maximum detected strain in the formed PLC bands is approximately 0.025 and it is very close to the uniaxial condition. Moreover, the strain localization during biaxial stretching is observed always at the same region. When strain localizations are examined, higher amounts are observed near the edge of gage, where it is twice the strain accumulated at the center.

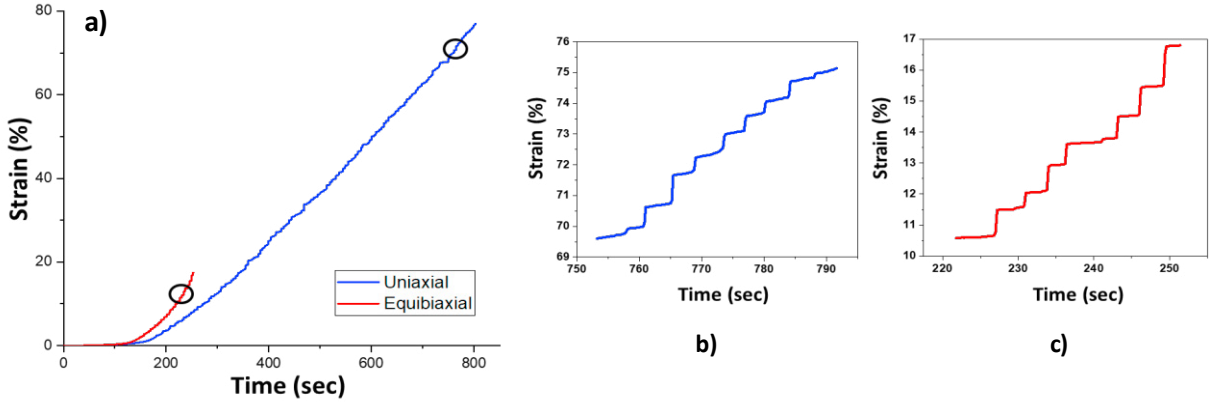

Fig. 5. (a) Strain versus time plot of the material during uniaxial and equibiaxial stretching (b) zoomed view of the circle in uniaxial region (c) zoomed view of the circle in biaxial region.

Strain-time plots of the material during testing do not show linear behavior as shown in Fig. 5a. Curves are also serrated due to the strain jumps from PLC bands. Slopes of the curves after elastic deformation are also different and strain-time plot of biaxial testing shows a steeper strain rise with time compared to the uniaxial condition. Fig. 5b and 5c give the strain changes from each PLC band clearly. For a given time interval, the number of strain jumps under uniaxial loading is higher than the biaxial condition, highlighting the importance of strain path for PLC formation. Under shear dominated stress state (uniaxial stretching), PLC effects seem to be clearer. Average strain jump under uniaxial stretching is 0.0055 while it is 0.0059 under biaxial stretching. Towards the end of the test, PLC bands cross each other in biaxial condition, resulting in higher strain jumps than usual. The strain increase between two successive bands is only 0.001 under both uniaxial and biaxial conditions.

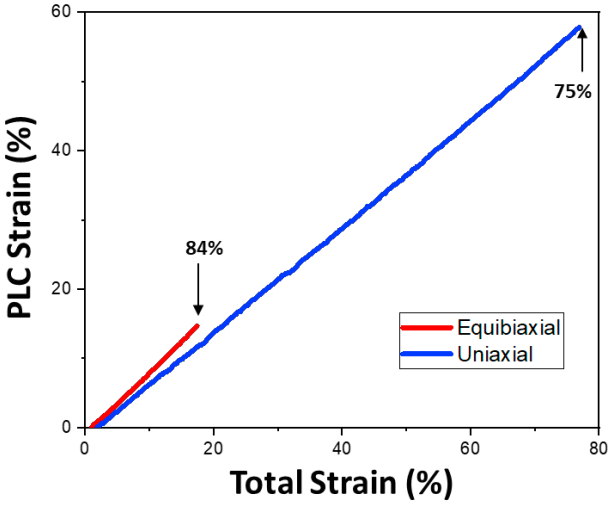

Fig. 6. Strain contribution of PLC bands versus total strain graph under uniaxial and biaxial condition (along ε_{xx} direction).

Fig. 6 represents the strain contribution of PLC bands to overall deformation. The contribution of all stain jumps to the overall deformation in biaxial and uniaxial condition are 84% and 75%, respectively. Since the negative effects of the PLC bands in the deformation, such as negative strain rate sensitivity, lower formability and poor surface finish, are known; the higher PLC contribution in biaxial stretching is expected to affect the material more negatively. However, the load-time and load-strain graphs showed that the formability was unaffected with the strain path change (Fig. 3). Under both conditions, material deformed until typical fracture strains. Therefore, even the majority of strain is localized to the PLC bands under both conditions; the overall formability does not depend on them significantly.

Besides the strain heterogeneity, a more significant drawback of the PLC bands is the formation of shear bands. Under uniaxial tension, the repetitive formation of PLC bands in a particular region of the sample leads to a shear band at the same region (Fig. 7a). PLC bands create nucleation sites for the shear bands and this is also observed by Kang et al. (2008) and Yoshida and Toyooka (2001). Shear stress state in uniaxial case promotes full-scale PLC bands that stretch through the whole gage length, whereas in biaxial they form only to a limited extent because global shear stresses are zero (Fig. 4). The local resolved shear stresses cause slip and therefore PLC bands in biaxial case, however they do not grow fully. In uniaxial case, on the other hand, a collection of full-scale PLC bands in the same region of the sample avalanche into a shear band, where further shear strains accumulate (Fig. 7a). A single shear band in uniaxial contains multiple PLC bands that appear as surface irregularities in Fig. 7a. The shear bands then cross each other, which also causes catastrophic failure from the same regions. Conversely, there are no surface irregularities or shear bands observed on the surface after biaxial deformation. Fracture surfaces shown in Fig. 7b prove that the fracture and deformation mode of the uniaxial tension is shear-based and relatively brittle. Shear bands formed due to the PLC bands result in elongated sharp dimples. The fracture surface after biaxial stretching has a typical ductile fracture structure with round dimples (Fig. 7c).

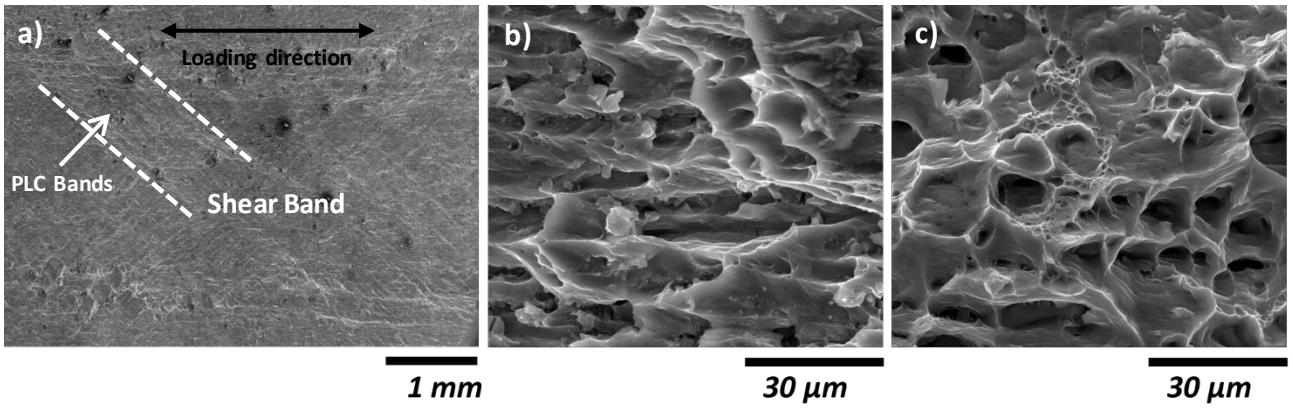

Fig. 7. SEM images of (a) formed shear bands after uniaxial tension, (b) fracture surface after uniaxial tension, and (c) fracture surface after biaxial tension.

EBSD analysis shows the deformation microstructures and textures for both strain paths at a constant equivalent strain, ε_{eq} = 0.18. In biaxial stretching, deformation texture is brass (Fig. 8 and b), parallel to the observations in literature (Banovic and Foecke (2003)). The brass texture is not far off from the initial copper texture. In uniaxial condition, on the other hand, an increase in cube component of the texture is obvious. The initial copper texture evolves into a cube texture after sufficient deformation as shown in Fig. 8c and 8d. Therefore, it is once again proved that the shear bands dominate the deformation in uniaxial condition. Since the cube texture component is a result of shear-based deformation in aluminum alloys, the increase in this texture component explains the relationship between PLC and shear bands. The texture change in the material is not due to a single PLC band, but rather a collection of them, which evolve into the shear bands. The combination of the shear bands with the strain path is responsible from the significant change in texture.

The cube component of the uniaxial condition is clearer when the EBSD analysis was done on the formed shear band shown in Fig. 9. The EBSD result from the shear band contains many black spots, where the diffraction quality was poor. This is due to the high deformation amounts ($\varepsilon > 0.3$) within the band, which limits the quality of the data. However, the remaining data is enough to confirm that the {001}<100> texture component is activated in uniaxial loading due to the shear bands. Lack of full-scale PLC bands and the shear bands in biaxial stretching prevents this kind of texture change and keeps the initial texture with minor changes.

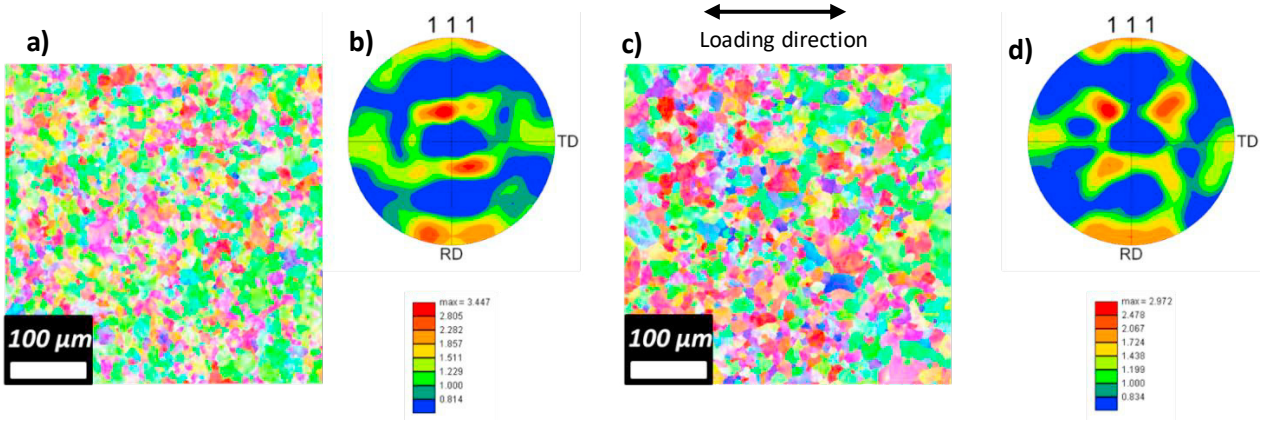

Fig. 8. EBSD analysis of the specimen (a) grain orientation map (b) 111 pole figure after equibiaxial loading, (c) grain orientation map (d) 111 pole figure after uniaxial loading.

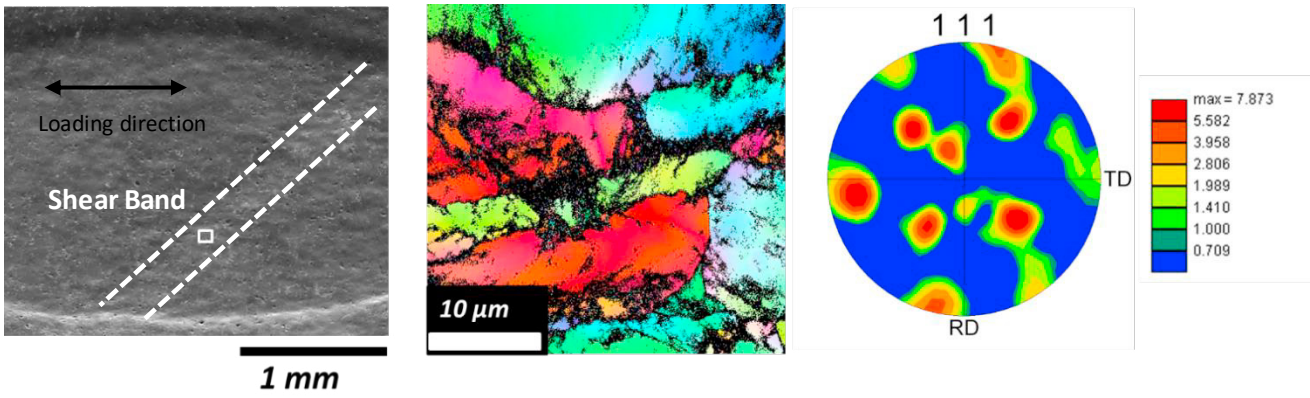

Fig. 9. EBSD analysis from the first formed shear band in uniaxial stretching.

4. Conclusions

Considerable PLC activity is present under both uniaxial and biaxial loading, where the PLC bands sustain the majority of overall strain. While the deformation is heterogeneous with jerky load response, PLC bands do not change the overall formability of the material. However, shear stresses in uniaxial loading promote full-scale, sharp PLC bands stretching through the whole gage length of the samples. The repetitive, sharp PLC bands evolve into the shear bands, which act as stress concentrators and result in shear-based and catastrophic fracture (elongated dimples) of the samples. The deformation texture also has shear-based, cube-{001}<100> type components under uniaxial loading. On the other hand, the shear bands are suppressed under biaxial tension due to the lack of well-defined, sharp PLC bands. The samples are devoid of surface irregularities and fail by typical ductile fracture. There is also a slight change in the final texture. Therefore, the biaxial strain path seems to be more favourable for higher quality final products of materials demonstrating PLC behavior.

Acknowledgements

This work was supported by European Commission's Research Executive Agency's Marie Skłodowska-Curie Actions – Career Integration Grant (FP7-PEOPLE-2013-CIG) with grant agreement #631774.

References

Cottrell., A.H., 1953. Theory of dislocations. Progress in Metal Physics 4, 205-264.

Ait-Amokhtar, H., Fressengeas, C., 2010. Crossover from continuous to discontinuous propagation in the Portevin-Le Chatelier effect. Acta Materialia, 58(4), 1342–1349.

Antolovich, S. D., & Armstrong, R. W. (2014). Plastic strain localization in metals: Origins and consequences. Progress in Materials Science, 59(1), 1–160.

Banovic, S. W., Foecke, T., 2003. Evolution of strain-induced microstructure and texture in commercial aluminum sheet under balanced biaxial stretching. Metallurgical and Materials Transactions A: Physical Metallurgy and Materials Science, 34 A(3), 657–671.

Beaudoin, A., Wilkinson, D., Embury, J., Jain, M., Sachdev, A., Kang, J., Kim, S., 2005. On the sequence of inhomogeneous deformation processes occurring during tensile deformation of strip cast AA5754. Acta Materialia, 54(1), 209–218.

Cai, Y. L., Yang, S. L., Wang, Y. H., Fu, S. H., & Zhang, Q. C., 2016. Characterization of the deformation behaviors associated with the serrated flow of a 5456 Al-based alloy using two orthogonal digital image correlation systems. Materials Science and Engineering A, 664, 155–164.

Chatterjee, A., Murty, K. L., Gayathri, N., Mukherjee, P., Barat, P., 2011. Temperature dependence of the dynamics of Portevin-Le Chatelier effect in Al-2.5 Pct Mg Alloy. Metallurgical and Materials Transactions A: Physical Metallurgy and Materials Science, 42(5), 1184–1190.

Clausen, A. H., Børvik, T., Hopperstad, O. S., Benallal, A., 2004. Flow and fracture characteristics of aluminium alloy AA5083-H116 as function of strain rate, temperature and triaxiality. Materials Science and Engineering A, 364(1–2), 260–272.

Güler, B., Efe, M., 2018. Forming and fracture limits of sheet metals deforming without a local neck. Journal of Materials Processing Technology, 252(February 2017), 477–484.

Hamasaki, H., Tamashiro, F., 2018. Biaxial deformation on AA5182-O aluminium alloy sheet at warm temperature. Journal of Physics: Conference Series 1063(1), 012032, 1-5.

Hertzberg, R. W., Hauser, F. E., 2010. Deformation and Fracture Mechanics of Engineering Materials. Journal of Engineering Materials and Technology.

Hirsch, J., Al-Samman, T., 2013. Superior light metals by texture engineering: Optimized aluminum and magnesium alloys for automotive applications. Acta Materialia 61(3), 818–843.

Hou, Y., Min, J., Lin, J., Carsley, J. E., Stoughton, T. B., 2018. Plastic instabilities in AA5754-O under various stress states. IOP Conference Series: Materials Science and Engineering 418(1), 012050, 1-8.

Iadicola, M. A., Foecke, T., Banovic, S. W., 2008. Experimental observations of evolving yield loci in biaxially strained AA5754-O. International Journal of Plasticity 24(11), 2084–2101.

Iadicola, M. A., Hu, L., Rollett, A. D., Foecke, T., 2011. 5754 aluminum sheet deformed along Bi-linear strain paths. AIP Conference Proceedings 1383(2011), 299–306.

Jiang, H., Zhang, Q., Chen, X., Chen, Z., Jiang, Z., Wu, X., Fan, J., 2007. Three types of Portevin-Le Chatelier effects: Experiment and modelling. Acta Materialia 55(7), 2219–2228.

Jiang, H., Zhang, Q., Wu, X., Fan, J., 2006. Spatiotemporal aspects of the Portevin-Le Chatelier effect in annealed and solution-treated aluminum alloys. Scripta Materialia 54(12), 2041–2045.

Kang, J., Wilkinson, D. S., Bruhis, M., Jain, M., Wu, P. D., Embury, J. D., Sachdev, A. K., 2008. Shear localization and damage in AA5754 aluminum alloy sheets. Journal of Materials Engineering and Performance 17(3), 395–401.

Le Cam, J. B., Robin, E., Leotoing, L., Guines, D., 2017. Calorimetric analysis of Portevin-Le Chatelier bands under equibiaxial loading conditions in Al–Mg alloys: Kinematics and mechanical dissipation. Mechanics of Materials 105, 80–88.

McCormick, P. G., (1971). The Portevin-Le Chatelier effect in an Al-Mg-Si alloy. Acta Metallurgica 19.5, 463-471.

Min, J., Hector, L. G., Carsley, J. E., Stoughton, T. B., Carlson, B. E., Lin, J., 2015. Spatio-temporal characteristics of plastic instability in AA5182-O during biaxial deformation. Materials and Design 83, 786–794.

Motsi, G. T., Olubambi, P. A., Sono, T. J., Shoke, L., 2014. In Situ Electron Microscopy Studies on the Tensile Deformation Mechanisms in Aluminium 5083 Alloy. Advanced Materials Research 1019, 103–111.

Mulford, R. A., Kocks, U. F., 1979. New observations on the mechanisms of dynamic strain aging and of jerky flow. Acta Metallurgica.

Saad, G., Fayek, S. A., Fawzy, A., Soliman, H. N., Nassr, E., 2010. Serrated flow and work hardening characteristics of Al-5356 alloy. Journal of Alloys and Compounds 502(1), 139–146.

Sene, N. A., Balland, P., Bouabdallah, K., 2018. Experimental study of Portevin–Le Châtelier bands on tensile and plane strain tensile tests. Archives of Civil and Mechanical Engineering 18(1), 94–102.

Seymen, Y., Güler, B., Efe, M., 2016. Large Strain and Small-Scale Biaxial Testing of Sheet Metals. Experimental Mechanics 56(9), 1519–1530.

Shibkov, A. A., Zheltov, M. A., Gasanov, M. F., Zolotov, A. E., 2018. Dynamics of a Lüders Band and Destruction of an Aluminum-Magnesium Alloy, Initiated by a Stress Concentrator. Physics of the Solid State 60(2), 320–327.

Shuklinov, A. V., Denisov, A. A., Zheltov, M. A., Zolotov, A. E., Shibkov, A. A., 2011. Dynamics of deformation bands and fracture of the aluminum-magnesium alloy 5556. Physics of the Solid State 53(10), 1975–1980.

Sleeswyk, A. W. 1958. Slow strain-hardening of ingot iron. Acta Metallurgica 6 (9), 198-603.

Song, X., Leotoing, L., Guines, D., Ragneau, E., (2016). Investigation of the forming limit strains at fracture of AA5086 sheets using an in-plane biaxial tensile test. Engineering Fracture Mechanics 163, 130–140.

Tian, N., Wang, G., Zhou, Y., Liu, K., Zhao, G., Zuo, L., 2018. Study of the Portevin-Le Chatelier (PLC) characteristics of a 5083 aluminum alloy sheet in two heat treatment states. Materials 11(9), 1533, 1-16.

Wen, W., Zhao, Y., Morris, J. G., 2005. The effect of Mg precipitation on the mechanical properties of 5xxx aluminum alloys. Materials Science and Engineering A 392(1–2), 136–144.

Yilmaz, A., 2011. The Portevin-Le Chatelier effect: A review of experimental findings. Science and Technology of Advanced Materials, 12(6).

Yoshida, S., Toyooka, S., 2001. Field theoretical interpretation on dynamics of plastic deformation-Portevin-Le Chatelie effect and propagation of shear band. Journal of Physics Condensed Matter 13(31), 6741–6757.

Yuzbekova, D., Mogucheva, A., Zhemchuzhnikova, D., Lebedkina, T., Lebyodkin, M., Kaibyshev, R., 2017. Effect of microstructure on continuous propagation of the Portevin-Le Chatelier deformation bands. International Journal of Plasticity 96, 210–226.

Zhemchuzhnikova, D., Lebyodkin, M., Yuzbekova, D., Lebedkina, T., Mogucheva, A., Kaibyshev, R., 2018. Interrelation between the portevin le-chatelier effect and necking in almg alloys. International Journal of Plasticity 110(June), 95–109.